# Title Page

**Title:** Comprehensive analysis of pyroptosis-associated in molecular classification, immunity and prognostic of glioma

**Running head**: Pyroptosis and glioma

**Authors and affiliations**

Peng Chen[1], Yanyan Li[3], Na Li[2], Liangfang Shen[2], Zhanzhan Li[2*]

Peng Chen, chenpengsurgery@hotmail.com, Department of orthopedics, Xiangya Hospital, Central South University, Changsha, Hunan Province 410008, China

Yanyan Li, liyan4005@126.com, Department of Nursing, Xiangya Hospital, Central South University, Changsha, Hunan Province 410008, China

Na Li, 21739082@qq.com, Department of Oncology, Xiangya Hospital, Central South University, Changsha, Hunan Province 410008, China.

Liangfang Shen, liangfangshen86@126.com, Department of Oncology, Xiangya Hospital, Central South University, Changsha, Hunan Province 410008, China.

Zhanzhan Li*, lizhanzhan@csu.edu.cn, Department of Oncology, Xiangya Hospital, Central South University, Changsha, Hunan Province 410008, China.

***Correspondence to:** Zhanzhan Li, No.87, Xiangya Road, Kaifu District, Changsha, Hunan Province 410008, China. **E-mail:** lizhanzhan@csu.edu.cn

## Abstract

Integrative analysis was performed in the Chinese Glioma Genome Atlas and The Cancer Genome Atlas to describe the pyroptosis-associated molecular classification and prognostic signature in glioma. Pyroptosis-related genes were used for consensus clustering and to develop a prognostic signature. The immune statuses, molecular alterations and clinical features of differentially expressed genes were analyzed among different subclasses and risk groups. A lncRNA-miRNA-mRNA network was built, and drug sensitivity analysis was used to identify small molecular drugs for the identified genes. Glioma can be divided into two subclasses using 30 pyroptosis-related genes. Cluster 1 displayed high immune signatures and poor prognosis as well as high immune-related function scores. A prognostic signature based on 15 pyroptosis-related genes of the CGGA cohort can predict the overall survival of glioma and was well validated in the TCGA cohort. Cluster 1 had higher risk scores. The high-risk group had high immune cell and function scores and low DNA methylation of pyroptosis-related genes. The differences in pyroptosis-related gene mutations and somatic copy numbers were significant between the high-risk and low-risk groups. The ceRNA regulatory network uncovered the regulatory patterns of different risk groups in glioma. Nine pairs of target genes and drugs were identified. In vitro, CASP8 promotes the progression of glioma cells. Pyroptosis-related genes can reflect the molecular biological and clinical features of glioma subclasses. The established prognostic signature can predict prognosis and distinguish molecular alterations in glioma patients. Our comprehensive analyses provide valuable guidelines for improving glioma patient management and

individualized therapy.

**Keywords:** Glioma, pyroptosis, prognostic signature, Tumor immunity, clinical nomogram

## INTRODUCTION

Gliomas are the most common types of primary tumors in the central nervous system and one of the most devastating tumors(1). At present, the main treatment methods of glioma are surgical resection, radiotherapy, chemotherapy or chemoradiotherapy(2). Although great efforts have been made to improve glioma treatment, the prognosis of glioma patients remains poor(3). One of the main reasons is that the molecular mechanism is still not fully understood. Therefore, the exploration and research of the underlying mechanism of gliomas and identification of potential treatment targets followed by application in clinical practice have important theoretical and practical significance.

Pyroptosis is one of the pathways involved in programmed cell death, such as apoptosis, ferroptosis, necroptosis, and autophagy.(4) Cookson et al. first used pyroptosis to describe the caspase-1-dependent pattern of cell death found in macrophages(5). Pyroptosis, distinct from apoptosis and necrosis, contributes to a range of human diseases as a new mechanism of cell death. Pyroptosis is a proinflammatory form of programmed cell death that is dependent on the activity of caspase acid-specific proteases(6). In the coupling of the amino-terminal and carboxy-terminal linkers of gasdermin D (GSDMD) by caspases, the latter is displaced onto the membrane and perforated, inducing moisture penetration, cell swelling and the release of inflammatory

factors, which is followed by pyroptosis(7). A previous study reported that pyroptosis plays an important role in immunity and diseases. Pyroptosis can promote the death of damaged cells during infection and acts as an alarm signal for the recruitment of immune cells to the site of infection to promote the removal of pathogens, thus effectively protecting the body(8). In recent years, its role in tumorigenesis and cancer development has been studied comprehensively. Various regulators have been reported to be involved in the process of pyroptosis and play pivotal roles in the progression of tumors, such as hepatocellular carcinoma, lung cancer, and breast cancer(9-11). However, few studies have investigated the role of pyroptosis in glioma, and comprehensive analyses of pyroptosis regulators in glioma, their correlation with clinical characteristics and their prognostic value have not been reported.

In the present study, we first outlined the molecular subtypes of gliomas based on pyroptosis-related genes in the CGGA dataset and described the clinical and molecular characteristics and immune status of each subclass. Then, we developed a prognostic signature of pyroptosis-related genes based on the CGGA cohort, validated this prognostic signature in the TCGA cohort. Furthermore, we explored the clinical and molecular patterns, including immune infiltration, somatic copy number alterations, mutations, and DNA methylation, and established a lncRNA-miRNA-mRNA regulatory network. Finally, we explored the correlation between small molecular drugs and the identified prognostic signature genes. Our comprehensive analyses provide new insight into the functions of pyroptosis in the initiation, development, and progression of glioma.

## MATERIALS AND METHODS

### Data source

We downloaded the genomic data, copy number alteration, methylation and clinical data of glioma patients from the CGGA (http://www.cgga.org.cn/) and TCGA databases (https://portal.gdc.cancer.gov/). Additional gene-centric RMA-normalized gene expression profiles and drug response data of over 1000 cancer cell lines were accessed from the Genomics of Drug Sensitivity in Cancer (GDSC) database (https://www.cancerrxgene.org/downloads). Immune-associated data, including immune cells and immunophenoscores, were downloaded from TCIA (https://tcia.at/home). Thirty-three pyroptosis-related genes were defined from a previous publication and are provided in Table S1(12-15).

### Identification of glioma subclasses and Gene set variation analysis

We identified the optimal clustering number visualizing consensus matrix, tracking plot, and cumulative distribution function plot. In addition, a T-distributed stochastic neighbor embedding-based approach was used to validate the clustering in glioma patients. We calculated the enrichment scores for every sample using the GSVA R package.

### Development and validation of a prognostic signature

We developed a pyroptosis-related prognostic signature based on the CGGA training cohort. Twenty differentially expressed genes with $P<0.05$ were entered into LASSO Cox regression, which identified potential genes for the prognostic signature in the CGGA training cohort. Then, we calculated the risk score for each sample of the CGGA

and TCGA validation cohorts using the obtained regression coefficient in the CGGA training cohort: risk score =coef1*$gene_1$ expression+$coef_2$* $gene_2$ expression+…$coef_n$*$gene_n$ expression. The CGGA and TCGA samples were divided into a high-risk group and a low-risk group based on the median risk score. Receiver operating characteristic curves were plotted to evaluate the 1-year, 2-year, and 3-year sensitivity and specificity of the prognostic signature. We also established a prognostic nomogram to evaluate the clinical value of the prognostic signature. Calibration analysis of the prognostic predictive value of the nomogram was carried out.

**Functional enrichment analysis, estimation of tumor stem cell-like properties and immune infiltration**

Gene Ontology and KEGG pathway analyses were performed using the "clusterProfiler" package. We used single-sample gene set enrichment analysis (ssGSEA) to estimate the enrichment score of stem cell-like properties (RNAss, DNAss) and the TME (stromal score, immune score, and ESTIMATE score) in the TCGA cohort because the CGGA dataset did not provide such data. The immune-related cell and function scores were also calculated for each sample (downloaded from https://www.gsea-msigdb.org/).

**Somatic copy number alteration, mutation, and DNA methylation analysis**

Based on the risk groups in the TCGA cohort, we compared the somatic copy number alteration, mutation, and DNA methylation levels between the high-risk and low-risk groups using the "limma" R package.

**Construction of a ceRNA network and drug sensitivity**

To further explore the transcriptome regulation network of different risk groups, we

used Cytoscape version 3.8.2 to establish a lncRNA-miRNA-mRNA regulatory network. We explore the correlation between small molecular drugs and the identified prognostic signature genes using Pearson correlation analysis |R|>0.25 and P>0.05 were considered significant.

**Verification of experiments in vitro**

We further performed the Western blot, cell migration assays, cell scratchy assays, and clonogenic assays to verify the present finding. We selected the CASP8 to validate the molecular function because CASP8 showed significant differences between normal tissue and GBM or LGG, and the elevated expression is associated with poor prognosis. The details of experiments process in vitro were supplied in Additional file 1.docx.

**Statistical analysis**

The log-rank test was used to compare the survival curves of Kaplan-Meier analysis. The hazard ratio (HR) and 95% confidence interval (CI) of each gene and clinical parameters were calculated when univariate and multivariate Cox regression were applied. All analyses were achieved using R software version 4.0. A two-sided P value <0.05 was considered significant unless otherwise specified.

**RESULTS**

**Identification of glioma subclasses**

The flow chart of the data analysis is presented in Figure 1A. From two CGGA RNA-seq datasets, we obtained 1018 samples of gene expression data and further identified 30 pyroptosis-related genes based on MAD>0.5. The gene symbols and descriptions of the 30 pyroptosis-associated genes used for classification are listed in the Additional

file 2: Table S1. We first explored the interactions among these genes using PPIs (Figure 1B), and the PPI network indicated that CASP8, CASP4, CASP1, NLRP3, NLRP1 and NLRC4 are hub genes. The correlation circle plot of the 30 genes is presented in Figure 1C (red: positive correlation; green: negative correlation). We identified the optimal k value as 2 by estimating the comprehensive correlation coefficient. Therefore, we divided the glioma samples into two different subclasses: cluster 1 and cluster 2. For the optimal k value (k=2), the consensus matrix showed a relatively sharp and clear boundary, indicating stable and robust clustering (Figure 1D). To verify the subclass stability, we further performed t-sensitivity PCA and found that a two-dimensional t-sensitivity distribution supported subtype clustering (Figure 1E). The consensus clustering for each sample is listed in Additional file 2: Table S2. The Kaplan-Meier analysis indicates that the median survival time was significantly shorter in cluster 2 than in cluster 1 (MST: 1.87 vs. 6.92 years, $P<0.001$, Figure 1F). This result indicated that the two subclasses had distinct prognostic patterns.

**Correlation of glioma subclasses with pyroptosis-related genes**

Two subclasses were obtained based on pyroptosis-related genes. To explore the pathway enrichment for the two subclasses, we performed GSVA by transforming the expression data from a gene-by-sample matrix to a gene set by two subclasses. Then, differential pathways were enriched in the two subclasses. Compared with cluster 1, the GSVA results indicated that cluster 2 had 182 kinds of significantly differential signaling pathways (Additional file 2: Table S3). The upregulated pathways were associated with immune-related pathways, such as autoimmune, allograft rejection,

177 graft versus host disease, primary immunodeficiency, antigen processing and
178 presentation. Some signaling pathways, such as the cytosolic DNA sensing pathway,
179 NOD-like receptor signaling pathway, Toll-like receptor signaling pathway, and
180 metabolism-related pathways, were also significantly enriched. The significantly
181 downregulated pathway was long-term potentiation (Figure 2A).

182 **Clinical characteristics and transcriptomes of glioma subclasses**

183 We explored the correlation of subclasses with clinical characteristics (Figure 2B).
184 Compared with patients in cluster 2 with a favorable prognosis, patients in cluster 1
185 tended to have GBM ($P<0.001$), WHO grade IV ($P<0.001$), a higher proportion of
186 age >41 years, 1p19q non-codeletion status ($P<0.001$), and IDH wildtype status
187 ($P<0.001$). Sex, PRS type and radiotherapy status were not associated with the
188 molecular subclasses ($P>0.05$). For the pyroptosis-related genes except CASP9,
189 significant differential expression was observed in the two clusters. Among these
190 differentially expressed genes, all genes were upregulated in cluster 1 and
191 downregulated in cluster 2 (Figure 2B). We also compared the differences in pyroptosis-
192 related genes in patients with different histologies, grades, IDH mutation statuses, and
193 1p19q statuses. Compared with the LGG group, the GBM group had one upregulated
194 gene (AIM2) and 21 downregulated genes (Additional file 3: Figure S1A). Twenty-one
195 DEGs were found for grade, and their expression increased with increasing WHO grade
196 ($P<0.005$, Additional file 3: Figure S1B). For IDH status, 25 DEGs were found
197 (Additional file 3: Figure S1C). Thirty pyroptosis-related DEGs were found for 1p191
198 status (Additional file 3: Figure S1D).

We further performed differential expression analysis between cluster 1 and cluster 2. A total of 392 DEGs were found, 18 genes were upregulated, and 372 genes were downregulated in cluster 2 (Additional file 2: Table S4). GO and KEGG enrichment analyses were performed for all DEGs (Additional file 2: Table S5 and Table S6). A total of 874 differentially expressed functions were enriched, including 709 biological processes, 95 cellular components and 70 molecular functions. The top 30 enrichment results are presented in Additional file 3: Figure S2. Most of these functions were associated with immunity. In addition, 56 pathways were also identified in the KEGG analysis (Additional file 3: Figure S3), and the top five pathways were phagosome, Staphylococcus aureus infection, tuberculosis, complement and coagulation cascades, and human T-cell leukemia virus 1 infection.

**Correlation of glioma subclasses with immune status**

To explore the tumor heterogeneity between the two subclasses, we investigated the immune cell and immune function differences. Compared with cluster 2, cluster 1 had higher aDC, CD8+ T cell, DC, iDC, macrophage, mast cell, neutrophil, NK cell, pDC, T helper cell, Tfh cell, Th2 cell, TIL, and Treg levels (all $P<0.001$, Additional file 3: Figure S4A). Similarly, cluster 1 had higher immune function scores than cluster 2, including APC coinhibition, APC costimulation, CCR, checkpoint, cytolytic activity, HLA, inflammation promotion, MHC class I, parainflammation, T cell coinhibition, type I IFN response and type II IFN response (all $P<0.001$, Additional file 3: Figure S4B).

**Development of a pyroptosis-related prognostic signature in glioma**

Initially, we performed univariate Cox regression to identify the correlations of the 30 pyroptosis-related genes with OS (Additional file 3: Figure S5A) in the CGGA cohort. In total, 20 pyroptosis-related genes were identified as associated with the overall survival of glioma patients. The Kaplan-Meier plot indicated that high expression of CASP3, CASP4, CASP5, CASP6, CASP8, ELANE, GSMAD, IL6, NLRP3, NOD1, NOD2, PLCG1, PRKACA, PYCARD, and SCAF11 was associated with poorer OS in glioma. Using 20 prognostic pyroptosis-related genes, we developed a prognostic signature by performing LASSO regression in the CGGA training cohort (Additional file 3: Figure S5B and S5C). Fifteen of the 20 prognostic genes were used to develop the risk signature. We calculated the risk score for each sample using the regression coefficients of the 15 genes (Additional file 2: Table S7). Glioma patients with risk scores greater than the median value were divided into a high-risk group, and the others were divided into a low-risk group. Compared with the low-risk group, the high-risk group was more likely to have GBM ($P<0.001$), a higher WHO grade ($P<0.001$), recurrence ($P<0.001$), older age ($P<0.001$), IDH wildtype status ($P<0.001$), 1p19q non-codeletion status ($P<0.001$), and a history of chemotherapy ($P<0.001$). The heatmap showed the association between the risk group and clinical parameters and differentially expressed genes of the high- and low-risk groups (Additional file 3: Figure S5D). Furthermore, we found that glioma patients belonging to cluster 1, patients with a poor prognosis, patients with GBM, patients with WHO grade IV patients with 1p19q non-codeletion status and patients with IDH wildtype status had higher risk scores (all $P<0.001$, Additional file 3: Figure S6).

The Kaplan-Meier analysis showed that the high-risk group had a significantly poorer OS than the low-risk group (Figure 3A-3 B). Univariate Cox regression indicated that the risk score was positively associated with OS in glioma (HR=3. 105, 95% CI: 2.681–3.596, P<0.001, Figure 3C). Multivariate Cox regression suggested that the risk score was an independent unfavorable prognostic predictor in glioma (HR=1.685, 95% CI: 1.392–2.039, P<0.001, Figure 3D). In addition, PRS type, tumor grade, and age were positively associated with OS. However, chemotherapy, wildtype IDH status, and 1p19q status were negatively associated with OS in the CGGA training cohort. The PCA plot indicated that patients in different risk groups were separated into obviously different clusters (Figure 3E). Time-dependent receiver operating characteristic analysis was performed to evaluate the predictability of the prognostic model. Our results showed that the AUCs at 1 year, 2 years, and 3 years were 0.717, 0.784 and 0.773 (Figure 3F), respectively. We further compared the OS status among different histology, IDH status, 1p19q codeletion status, and grade subgroups. The results showed that the OS of the high-risk group was still poorer than that of the low-risk group (Additional file 3: Figure S7, all P<0.001).

**External validation of the pyroptosis-related prognostic signature in glioma**

To further validate the prognostic value of the pyroptosis-related gene model, we also calculated the risk score of glioma patients in the TCGA cohort using the regression coefficients of the CGGA cohort. The Kaplan-Meier analysis indicated a significant correlation of the high-risk group with worse OS than the low-risk group (Figure 4A-4C). Univariate Cox regression showed that the risk score was significantly associated

with OS in the TCGA cohort (HR=2.084, 95% CI: 1.890-2.297, P<0.001, Figure 4D). In multivariate Cox regression, the risk score was also an independent prognostic indicator (HR=1.425, 95% CI: 1.247–1.629 P<0.001, Figure 4E). The PCA plot validated the high- and low-risk distribution of all glioma patients based on the TCGA cohort. Furthermore, the AUCs of the risk score were 0.844 at 1 year, 0.863 at 2 years, and 0.874 at 3 years (Figure 4F).

**Prognostic prediction models**

To further evaluate the clinical prediction value of the prognostic signature, we constructed a prognostic nomogram model based on multivariate Cox regression analysis that included all clinical parameters in the CGGA cohort The calibration curves indicated that the clinical nomogram model could precisely predict the 1-year, 3-year and 5-year OS of glioma patients (C-index=0.799). The predictive accuracy of this nomogram was well validated in the TCGA cohort (C-index=0.841, Figure 5).

**Functional enrichment and immune infiltration analyses based on the prognostic signature**

We further explored the underlying biological functions that define the survival of glioma patients. We first performed DEG analysis between the high-risk and low-risk groups and then annotated the functions of the DEGs in terms of biological processes, cellular components, and molecular functions using GO enrichment and KEGG pathways. We identified 338 DEGs in the CGGA cohort (Additional file 2: Table S8) and 2600 DEGs in the TCGA cohort (Additional file 2: Table S9). The GO enrichment and KEGG pathway analyses indicated that the CGGA and TCGA cohorts shared some

enrichment results, such as extracellular matrix organization, extracellular structure organization, immune response, ECM-receptor interaction, and cell adhesion molecules (Figure 6A-6D).

We also explored the differences in immune cells and immune functions based on the risk score in the CGGA (Figure 6E and Figure 6G) and TCGA datasets (Figure 6F and Figure 6H). As shown in the box plots, the immune cell score showed a similar trend in the CGGA and TCGA datasets. All immune cell scores were significantly upregulated in the high-risk group. The immune function differences of the different risk groups were the same in the CGGA and TCGA datasets (all $P<0.001$). All immune function scores were significantly upregulated in the high-risk group. Significant expression levels were also observed among different immune subtypes, which indicated that the glioma prognosis risk could be associated with immune status (Additional file 3: Figure S8). We also explored the correlation of the expression of target genes with cancer stem cell-like properties (RNAss, DNAss) and the TME (stromal score, immune score, and ESTIMATE score). We found that PCG1 was negatively associated with RNAss, the stromal score, the immune score, and the ESTIMATE score. SCAF11 was only negatively associated with DNAss. The rest of the genes showed positive correlations with RNAss, DNAss and the stromal, immune and ESTIMATE scores (Additional file 3: Figure S9).

**Molecular alterations of pyroptosis-related genes based on the prognostic signature**

Molecular alterations of pyroptosis-related genes were also evaluated based on

309 histology in the TCGA dataset. NLRP2, NLRP7, and PLCG1 were the only gene
310 alterations in LGG, and NLRP3, NLRP7, NLRP2, SCAF11, NOD1, PLCG1, NLRP1,
311 and CASP1 were gene alterations in GBM. All gene alterations were within 2% (Figure
312 7). The somatic copy number alteration analysis indicated significant differences
313 among the pyroptosis-related genes. Among these genes, the copy variation number
314 was significantly increased in GPX4, NLRP7, NLRP2, CASP3, CASP6, IL1B, CASP8,
315 IL6, AIM2, NLRP4, NLRP3, PRKACA, ELANE, SCAF11, CASP9, NOD1, and
316 PLCG1 and was significantly decreased in GSDMB, GSDMD, NLRP1, CASP9,
317 TIRAP, CASP1, CASP4, NOD2, CASP5, PYCARD, GSMDC, GSMDA, and IL18 in
318 the high-risk group. The DNA methylation levels of the pyroptosis-related genes were
319 also compared. The results showed that the overall DNA methylation levels were
320 significantly decreased in the high-risk group and increased in the low-risk group.

321 **Construction of a ceRNA network based on the prognostic signature**

322 A ceRNA network was constructed based on the differentially expressed mRNAs,
323 lncRNAs and miRNAs between the high-risk and low-risk groups in the TCGA dataset.
324 We identified 763 downregulated mRNAs, 1176 upregulated mRNAs, 116
325 downregulated lncRNAs, 132 upregulated lncRNAs (Additional file 2: Table S10), 47
326 downregulated miRNAs and 71 upregulated miRNAs (Additional file 2: Table S11).
327 Finally, 39 mRNAs (28 upregulated and 11 downregulated), 26 lncRNAs (15
328 upregulated and 15 downregulated) and 14 miRNAs (13 upregulated and 1
329 downregulated) were included in the ceRNA network (Figure 8). The Kaplan-Meier
330 curves suggested that 13 lncRNAs (positive correlation: AC025211.1, AC068643.1,

GDNF-AS1, and LINC00519; negative correlation: ADH1L1-AS2, CRNDE, FAM181A-AS1, HOTAIRM1, MCF2L-AS1, MIR210HG, NEAT1, SLC6A1, and SNHG9; Additional file 3: Figure S10), 41 mRNAs (Additional file 2: Table S12 and Additional file 3: Figure S11) and 8 miRNAs (miR-21, miR-155, miR-200a, miR-216a, miR-221, miR-222, miR-429, and miR-503; Additional file 3: Figure S12) were associated with OS in glioma patients.

**Drug sensitivity analysis**

To identify potential target drugs, we performed correlations of the identified prognostic signature genes with drugs. We identified 257 pairs of significant gene-drug correlations (Additional file 2: Table S13). There were 9 pairs with correlation coefficients >0.5 or <-0.5.

ELANE-hydroxyurea, ELANE-cyclophosphamide, CASP3-nelarabine, NOD2-imiquimod, NLRP3-rebimastat, ELANE-ABT-199, ELANE-imexon, and NOD2-isotretinoin showed drug sensitivity. PRKACA-cobimetinib showed drug resistance (Figure 9).

**CASP8 promotes the progression of glioma cells**

We selected the CASP8 to validate the molecular function because CASP8 showed significant differences between normal tissue and GBM or LGG in GTEx database (Additional file 3: Figure S13). We firstly detected the expression of CASP8 in glioma cell lines using the Western blot analysis, and found CASP8 is the most highly expressed in LN299 cell. We built the CASP8-si LN229, H4 and U87 cells of glioma. The qPCR indicated mRNA level of CASP8 is significantly down-regulated in U87 and

LN229 cells. Furthermore, the silence of CASP8 expression inhibited the cell migration ability (Figure 10). The clonogenic assay also showed that the number of clonogenicity of U87 and LN229 cells were significantly suppressed after knockout of CASP8. These results suggested that CASP8 promotes the progression of glioma cells.

## DISCUSSION

The traditional histologic-based classification has some limitations, although this classification system has been updated several times over the years and serves clinicians well. One of the primary limitations is interobserver variability(16). A previous study reported that the concordance for reviewing a case is only approximately 50% among different neuropathologists, especially for astrocytic glioma versus oligodendroglioma(17). The development of genomics has allowed us to better understand the differences in prognosis and molecular features and promote effective treatment in glioma subclasses based on molecular features. Using 30 pyroptosis-related genes, we divided glioma patients into two subtypes. Significant overall survival differences were observed between cluster 1 and cluster 2. GSVA indicated that cluster 1 was enriched in some immune-related pathways. Cluster 1 and cluster 2 showed absolute differences in immune cells and immune functions. The infiltration levels of all kinds of immune cells, except Th1 cells, were higher in cluster 1, which had a poor prognosis than in cluster 2. Cluster 1 also showed more significant trends in some main immune function levels, such as immune checkpoints, inflammation promotion, par inflammation. A recent study reported that pyroptosis presents antitumor immune function in tumors, namely, pyroptosis-induced inflammation triggers robust antitumor

375 immunity and can synergize with checkpoint blockade(18). Moreover, some key
376 pathways were also highly enriched in cluster 1, such as the NOD-like receptor
377 signaling pathway, Toll-like receptor signaling pathway, and cytosolic DNA sensing
378 pathway, which were reported to be involved in glioma progression(19-21). These
379 results indicated that pyroptosis-related genes divided glioma patients into two-
380 dimensional distributions well.

381 We established a prognostic signature based on 15 pyroptosis-related genes. This
382 prognostic signature was well validated in an external independent cohort, and in terms
383 of its predictability, AUCs of 0.844, 0.863, and 0.874 were achieved for 1, 2, and 3
384 years, respectively, which showed its high discernibility. Combining clinical features
385 and the risk score of the 15 genes, we developed a nomogram for clinical application.
386 The CGGA and TCGA datasets showed high consistency. These results indicated that
387 the prognostic signature based on pyroptosis-related genes has high clinical value.

388 The signature genes were involved in two biological mechanisms of pyroptosis. The
389 assembly of inflammasome bodies is the initial step of the classical pyroptosis pathway.
390 The inflammasome is a macromolecular protein complex in the cytoplasm necessary
391 for the occurrence of inflammation and can recognize dangerous signaling molecules
392 such as bacteria and viruses. The inflammasome is mainly composed of pattern
393 recognition receptors (PRRs), apoptosis-associated speck-like protein (ASC) and pro-
394 caspase-1 precursors(22). PRRs are receptor proteins responsible for recognizing
395 different signal stimuli in cells. They are mainly composed of nucleotide-binding
396 oligomerization domain-like receptor protein (NLRP) 1, NLRP3, nucleotide-binding

oligomerization domain-like receptor protein C4 (NLRC4), absent in melanoma 2 (AIM2) and other components(15). ASC is an adaptor protein that is mainly composed of the N-terminal pyrindomain (PYD) and the C-terminal caspase activation and recruitment domain (CARD)(23). Procaspase-1 is an effector molecule that can specifically cleave GSDMD after activation. After the danger signal sensor NLR1, NLRP3 or AIM2 recognizes the danger signal molecule, the N-terminal PYD is combined with the N-terminal PYD of the adaptor protein. ASC then recruits Caspase-1 through the interaction of the CARDCARD domain to complete the assembly of the inflamed body(24). This method of cell death mediated by Caspase-1 is called the classical pathway of pyroptosis(25). The non-classical pathway of pyrolysis is mainly mediated by Caspase-4, Caspase-5 and Caspase-11. After cells are stimulated by bacterial LPS, Caspases-4, -5, and -11 directly bind to bacterial LPS and are activated(26). Activated Caspases-4, -5, and -11 specifically cleave GSDMD and release the intramolecular inhibition of the GSDMD-N domain(27). The combination of the GSDMD-N-terminus and cell membrane phospholipids causes cell membrane pore formation, cell swelling and rupture and induces cell pyrolysis; the GSDMD-N-terminus can also activate Caspase-1 by activating the NLRP3 inflammasome(28). Activated Caspase-1 stimulates the maturation of IL-18 and IL-1β precursors, and IL-18 and IL-1β are secreted to the outside of the cell and amplify the inflammatory response. Yang et al found that in the nonclassical pathway that relies on Caspase-11, gap junction protein-1 (Pannexin-1) can be cleaved, and the cleavage of Pannexin-1 can activate its own channel and release ATP, which induces pyrolysis(29). Lamkanfi et al

found that in the nonclassical pathway that relies on Caspase-11, Pannexin-1 cleavage can also activate the NLRP3 inflammasome, which in turn activates Caspase-1 and induces the occurrence of pyroptosis(30). According to the results, mutations of pyroptosis-related genes are mainly attributed to the classical pathway of pyrolysis. More research is needed to validate the molecular mechanisms.

Based on the risk score, we classified glioma patients into high- and low-risk groups to discriminate clinical outcomes. We further explored the molecular features between the high- and low-risk groups. The functional enrichment analysis results were similar in the TCGA and CGGA datasets, and the same pathways appeared in the two datasets, such as ECM-receptor interaction, GABAergic synapse, focal adhesion, and extracellular matrix organization. The immune cells and immune functions showed similar trends: immune cell and functional scores were higher in the high-risk group. The clinical features showed that cluster 1 had a higher risk score and poorer prognosis than cluster 2. The results indicated that the classification was accurate and validated in the risk model. Furthermore, we compared the gene alterations, CNVs, and DNA methylation levels. Significantly different levels were observed, which reflected the different molecular features of the different risk groups. The ceRNA network identified several key lncRNA-miRNA-mRNA regulatory networks: FAM181A-AS1-miR-21-(CPEB3, SAIB1, BLC7A, MAP2K3, JAG1, TGFBI, FAM46A, SPRY2, and CALD1). The survival analysis further suggested the regulatory correlation: elevated FAM18A-AS1 and miR-21 were associated with poor prognosis in glioma, and low expression of BCL7A, SATB1 and CPEB3 was associated with favorable prognosis. Previous

experiments have reported the promoting role of miR-21 in glioma(31), and upregulation of SATB1 and CPEB3 is associated with the development and progression of glioma(32, 33). The drug sensitivity analysis indicated that NOD2, ELANE, CASP3, and PYCARD showed sensitivity to small molecular drugs, and PRKACA, IL6, and NLLRP3 showed resistance to some drugs. It was reported that the inhibition of the NLRP3 inflammasome by beta-hydroxybutyrate can suppress the migration of glioma cells(34). These results may provide some guidelines for clinical practice.

The present study indicated that pyroptosis-related genes can be used to classify glioma patients into two subclasses based on different molecular features and clinical characteristics. The established prognostic model based on 15 pyroptosis-related genes not only predicted the prognosis of glioma patients but also reflected the molecular alterations, immune infiltration statuses, and stem cell-like properties of different risk groups. The classification based on the risk score of prognostic signature genes revealed a lncRNA-miRNA-mRNA regulatory network. The correlation of signature genes with drug sensitivity may provide a rationale for clinical applications. Finally, our study provides a new understanding of pyroptosis in the development and progression of glioma and contributes new important insights for promoting glioma treatment strategies.

**Authors' contributions**

ZZL designed this study and directed the research group in all aspects, including planning, execution, and analysis of the study. LS drafted the manuscript. YYL, NL, YJZ, QZ collected the data. LZZ provided the statistical software, performed the data

463 analysis, YYL arranged the Figures and Tables. SLF revised the manuscript. All authors
464 have read and approved the final version of the manuscript.

465 **Funding**

466 This study was supported by the National Natural Science Foundation of China (No.
467 82003239), Hunan Province Natural Science Foundation (Youth Foundation Project)
468 (NO.2019JJ50945), and the Science Foundation of Xiangya Hospital for Young Scholar
469 (NO. 2018Q012).

470 **Conflict of Interest Statement**

471 The authors declare that they have no competing interests

472 **Data Availability Statements**

473 All data can be download from TCGA database (https://portal.gdc.cancer.gov/) and
474 CGGA (http://www.cgga.org.cn/)

475
476 **References**

477 1. Weller M, Wick W, Aldape K, Brada M, Berger M, Pfister SM, et al. Glioma.
478 *Nat Rev Dis Primers*. (2015) 1: 15017. doi:10.1038/nrdp.2015.17

479 2. Bush NA, Chang SM, Berger MS. Current and future strategies for treatment of
480 glioma. *Neurosurg Rev*. (2017) 40: 1-14. doi:10.1007/s10143-016-0709-8

481 3. Kan LK, Drummond K, Hunn M, Williams D, O'Brien TJ, Monif M. Potential
482 biomarkers and challenges in glioma diagnosis, therapy and prognosis. *BMJ Neurol*
483 *Open*. (2020) 2: e69. doi:10.1136/bmjno-2020-000069

484 4. Fink SL, Cookson BT. Apoptosis, pyroptosis, and necrosis: mechanistic
485 description of dead and dying eukaryotic cells. *Infect Immun*. (2005) 73: 1907-1916.

doi:10.1128/IAI.73.4.1907-1916.2005

5. Fink SL, Cookson BT. Caspase-1-dependent pore formation during pyroptosis leads to osmotic lysis of infected host macrophages. *Cell Microbiol*. (2006) 8: 1812-1825. doi:10.1111/j.1462-5822.2006.00751.x

6. Bergsbaken T, Fink SL, den Hartigh AB, Loomis WP, Cookson BT. Coordinated host responses during pyroptosis: caspase-1-dependent lysosome exocytosis and inflammatory cytokine maturation. *J Immunol*. (2011) 187: 2748-2754. doi:10.4049/jimmunol.1100477

7. Boise LH, Collins CM. Salmonella-induced cell death: apoptosis, necrosis or programmed cell death? *Trends Microbiol*. (2001) 9: 64-67. doi:10.1016/s0966-842x(00)01937-5

8. Fink SL, Cookson BT. Pillars Article: Caspase-1-dependent pore formation during pyroptosis leads to osmotic lysis of infected host macrophages. Cell Microbiol. 2006. 8: 1812-1825. *J Immunol*. (2019) 202: 1913-1926.

9. Hage C, Hoves S, Strauss L, Bissinger S, Prinz Y, Poschinger T, et al. Sorafenib Induces Pyroptosis in Macrophages and Triggers Natural Killer Cell-Mediated Cytotoxicity Against Hepatocellular Carcinoma. *Hepatology*. (2019) 70: 1280-1297. doi:10.1002/hep.30666

10. Lu C, Guo C, Chen H, Zhang H, Zhi L, Lv T, et al. A novel chimeric PD1-NKG2D-41BB receptor enhances antitumor activity of NK92 cells against human lung cancer H1299 cells by triggering pyroptosis. *Mol Immunol*. (2020) 122: 200-206. doi:10.1016/j.molimm.2020.04.016

11. An H, Heo JS, Kim P, Lian Z, Lee S, Park J, et al. Tetraarsenic hexoxide enhances generation of mitochondrial ROS to promote pyroptosis by inducing the activation of caspase-3/GSDME in triple-negative breast cancer cells. *Cell Death Dis*. (2021) 12: 159. doi:10.1038/s41419-021-03454-9

12. Karki R, Kanneganti TD. Diverging inflammasome signals in tumorigenesis and potential targeting. *Nat Rev Cancer*. (2019) 19: 197-214. doi:10.1038/s41568-019-0123-y

13. Xia X, Wang X, Cheng Z, Qin W, Lei L, Jiang J, et al. The role of pyroptosis in cancer: pro-cancer or pro-"host"? *Cell Death Dis*. (2019) 10: 650. doi:10.1038/s41419-019-1883-8

14. Wang B, Yin Q. AIM2 inflammasome activation and regulation: A structural perspective. *J Struct Biol*. (2017) 200: 279-282. doi:10.1016/j.jsb.2017.08.001

15. Man SM, Kanneganti TD. Regulation of inflammasome activation. *Immunol Rev*. (2015) 265: 6-21. doi:10.1111/imr.12296

16. Chen R, Smith-Cohn M, Cohen AL, Colman H. Glioma Subclassifications and Their Clinical Significance. *Neurotherapeutics*. (2017) 14: 284-297. doi:10.1007/s13311-017-0519-x

17. Coons SW, Johnson PC, Scheithauer BW, Yates AJ, Pearl DK. Improving diagnostic accuracy and interobserver concordance in the classification and grading of primary gliomas. *Cancer-Am Cancer Soc*. (1997) 79: 1381-1393. doi:10.1002/(sici)1097-0142(19970401)79:7<1381::aid-cncr16>3.0.co;2-w

18. Wang Q, Wang Y, Ding J, Wang C, Zhou X, Gao W, et al. A bioorthogonal

system reveals antitumour immune function of pyroptosis. *Nature*. (2020) 579: 421-426. doi:10.1038/s41586-020-2079-1

19. Huang Y, Zhang Q, Lubas M, Yuan Y, Yalcin F, Efe IE, et al. Synergistic Toll-like Receptor 3/9 Signaling Affects Properties and Impairs Glioma-Promoting Activity of Microglia. *J Neurosci*. (2020) 40: 6428-6443. doi:10.1523/JNEUROSCI.0666-20.2020

20. Saxena S, Jha S. Role of NOD- like Receptors in Glioma Angiogenesis: Insights into future therapeutic interventions. *Cytokine Growth Factor Rev*. (2017) 34: 15-26. doi:10.1016/j.cytogfr.2017.02.001

21. Giurdanella G, Motta C, Muriana S, Arena V, Anfuso CD, Lupo G, et al. Cytosolic and calcium-independent phospholipase A(2) mediate glioma-enhanced proangiogenic activity of brain endothelial cells. *Microvasc Res*. (2011) 81: 1-17. doi:10.1016/j.mvr.2010.11.005

22. Platnich JM, Muruve DA. NOD-like receptors and inflammasomes: A review of their canonical and non-canonical signaling pathways. *Arch Biochem Biophys*. (2019) 670: 4-14. doi:10.1016/j.abb.2019.02.008

23. Nambayan R, Sandin SI, Quint DA, Satyadi DM, de Alba E. The inflammasome adapter ASC assembles into filaments with integral participation of its two Death Domains, PYD and CARD. *J Biol Chem*. (2019) 294: 439-452. doi:10.1074/jbc.RA118.004407

24. Lu A, Magupalli VG, Ruan J, Yin Q, Atianand MK, Vos MR, et al. Unified polymerization mechanism for the assembly of ASC-dependent inflammasomes. *Cell*.

552 (2014) 156: 1193-1206. doi:10.1016/j.cell.2014.02.008

553 25. Case CL, Roy CR. Analyzing caspase-1 activation during Legionella

554 pneumophila infection in macrophages. *Methods Mol Biol*. (2013) 954: 479-491.

555 doi:10.1007/978-1-62703-161-5_29

556 26. Lagrange B, Benaoudia S, Wallet P, Magnotti F, Provost A, Michal F, et al.

557 Human caspase-4 detects tetra-acylated LPS and cytosolic Francisella and functions

558 differently from murine caspase-11. *Nat Commun*. (2018) 9: 242.

559 doi:10.1038/s41467-017-02682-y

560 27. Shi J, Zhao Y, Wang K, Shi X, Wang Y, Huang H, et al. Cleavage of GSDMD by

561 inflammatory caspases determines pyroptotic cell death. *Nature*. (2015) 526: 660-665.

562 doi:10.1038/nature15514

563 28. Kayagaki N, Stowe IB, Lee BL, O'Rourke K, Anderson K, Warming S, et al.

564 Caspase-11 cleaves gasdermin D for non-canonical inflammasome signalling. *Nature*.

565 (2015) 526: 666-671. doi:10.1038/nature15541

566 29. Yang D, He Y, Munoz-Planillo R, Liu Q, Nunez G. Caspase-11 Requires the

567 Pannexin-1 Channel and the Purinergic P2X7 Pore to Mediate Pyroptosis and

568 Endotoxic Shock. *Immunity*. (2015) 43: 923-932. doi:10.1016/j.immuni.2015.10.009

569 30. Lamkanfi M, Dixit VM. Mechanisms and functions of inflammasomes. *Cell*.

570 (2014) 157: 1013-1022. doi:10.1016/j.cell.2014.04.007

571 31. Hermansen SK, Nielsen BS, Aaberg-Jessen C, Kristensen BW. miR-21 Is Linked

572 to Glioma Angiogenesis: A Co-Localization Study. *J Histochem Cytochem*. (2016)

573 64: 138-148. doi:10.1369/0022155415623515

574 32. Chu SH, Ma YB, Feng DF, Zhang H, Zhu ZA, Li ZQ, et al. Upregulation of
575 SATB1 is associated with the development and progression of glioma. *J Transl Med*.
576 (2012) 10: 149. doi:10.1186/1479-5876-10-149
577 33. He Y, Nan H, Yan L, Ma T, Man M, Tian B, et al. Long non-coding RNA
578 MIR22HG inhibits glioma progression by downregulating microRNA-9/CPEB3.
579 *Oncol Lett*. (2021) 21: 157. doi:10.3892/ol.2020.12418
580 34. Shang S, Wang L, Zhang Y, Lu H, Lu X. The Beta-Hydroxybutyrate Suppresses
581 the Migration of Glioma Cells by Inhibition of NLRP3 Inflammasome. *Cell Mol*
582 *Neurobiol*. (2018) 38: 1479-1489. doi:10.1007/s10571-018-0617-2
583

584 **Figure legends**

585 **Figure 1** Identification of glioma subclasses using consensus clustering method in the
586 CGGA dataset. **(A)** Flow chart of the study. **(B)** PPI network indicating the interactions
587 among pyroptosis-related genes (interaction score=0.7). **(C)** The circle plot of
588 correlation among pyroptosis-related genes (green line: negative correlation, red line:
589 positive correlation). **(D)** Consensus matrix method clustering using 30 pyroptosis-
590 related genes. **(E)** PCA analysis showed the distribution of two glioma subclasses in the
591 CGGA dataset. **(F)** Overall survival curve of two clusters in the cohort.

592 **Figure 2** Characteristics of patients in cluster 1 and cluster 2 in CGGA cohort. **(A)**
593 Heatmap of gene set variation analysis of the pyroptosis-related genes from cluster 1
594 and cluster 2. **(B)** Heatmap showed the correlations between two subclasses and clinical
595 characteristics and differentially expressed pyroptosis-related genes in the CGGA

596 cohort.

597 **Figure 3** Establishment of a pyroptosis-related gene prognostic signature in the CGGA
598 cohort. **(A)** Kaplan-Meier curves for OS of patients in high- and low-risk group in
599 CGGA Cohort. **(B)** Distribution of risk score of all patients of CGGA cohort, and
600 Patients' survival time distribution. **(C)** Forest plot of univariate cox regression between
601 risk score and prognosis of glioma. **(D)** Forest plot of multivariate cox regression of
602 between risk score and prognosis of glioma. **(E)** PCA plot for signature genes based on
603 risk score group. **(F)** ROC curves showed the predictive efficiency of risk score at 1-
604 year, 2-year, 3-year point.

605 **Figure 4** External validation of a pyroptosis-related gene prognostic signature in the
606 TCGA cohort. **(A)** Kaplan-Meier curves for OS of patients in high- and low-risk group
607 in TCGA Cohort. **(B)** Distribution of risk score of all patients of TCGA cohort and
608 Patients' survival time distribution of TCGA cohort. **(C)** Forest plot of univariate cox
609 regression between risk score and prognosis of glioma in TCGA cohort. **(D)** Forest plot
610 of multivariate cox regression of between risk score and prognosis of glioma in TCGA
611 cohort. **(E)** PCA plot for signature genes based on risk score group in TCGA cohort. **(F)**
612 ROC curves showed the predictive efficiency of risk score at 1-year, 2-year, 3-year
613 point in TCGA cohort.

614 **Figure 5** Establishment and validation of nomogram model based on prognostic
615 signature genes. (A) Nomogram model established in the CGGA cohort. (B) The 1-year
616 calibration curves in the CGGA cohort. (C) The 3-year calibration curves in the CGGA
617 cohort. (D) The 5-year calibration curves in the CGGA cohort. (E) The 1-year

618 calibration curves in the TCGA cohort. (F) The 3-year calibration curves in the TCGA
619 cohort. (G) The 5-year calibration curves in the TCGA cohort.

620 **Figure 6** Functional enrichment and immune status analysis. **(A)** Barplot of enrichment
621 analysis based on prognostic-related signature genes in CGGA cohort. **(B)** Bubble plot
622 of enrichment analysis based on prognostic-related signature genes in CGGA cohort.
623 **(C)** Barplot of enrichment analysis based on prognostic-related signature genes in
624 TCGA cohort. **(D)** Bubble plot of enrichment analysis based on prognostic-related
625 signature genes in TCGA cohort. **(E)** Boxplot showed the ssGSEA scores for immune
626 cells based on risk group in CGGA cohort. **(F)** Boxplot showed the ssGSEA scores for
627 immune cells based on risk group in TCGA cohort. **(G)** Boxplot showed the ssGSEA
628 scores for immune pathways based on risk group in CGGA cohort. **(H)** Boxplot showed
629 the ssGSEA scores for immune pathways based on risk group in TCGA cohort

630 **Figure 7** Molecular alterations of pyroptosis-related genes in TCGA dataset. **(A)** The
631 mutations frequencies in low-risk group. **(B)** The mutations frequencies in high-risk
632 group. **(C)** Somatic copy number alteration based on risk groups. **(D)** DNA methylation
633 expression based on risk groups.

634 **Figure 8** The ceRNA network based on risk groups in TCGA dataset (red: up-regulation.
635 blue: down-regulation).

636 **Figure 9** Drug sensitivity analysis for identified prognostic-related genes based on
637 TCGA dataset (Top 16). **(A)** NOD2 and isotretinoin. **(B)** ELANE and Imexon. **(C)**
638 ELANE and ABT-199. **(D)** NLRP3 and Rebimastat. **(E)** NOD2 and Imuiquimod. **(F)**
639 CASP3 and Nelarabine. **(G)** ELANE and Cyclophosphamid. **(H)** ELANE and

Hydroxyurea. **(I)** PRKACA and Cobimetinib. **(J)** PRKACA and Rapamycin. **(K)** ELANE and Nandrolone. **(L)** PRKACA and Temsirolimus. **(M)** NOD2 and Eleschomol. **(N)** IL6 and geldanamycin. **(O)** IL6 and Lenvatinib. **(P)** PYCARD and Cyclophospharr

**Figure 10** CASP8 promotes progression of glioma cells. **(A)** The expression of CASP8 protein in human HA and glioma cell lines. **(B)** The western blot of CASP8 in U87, U1251, H4 cell lines after siRNA. **(C)** The mRNA expression level of CSAP8 in U87 and U251 after siRNA. **(D and E)** The scratch assay of CASP8-si in U87 and U251 cell lines. **(F and G)** Transwell assay of CASP8-si U87 and U251 cell lines. (H and I) The clonogenic assay of CASP8 in U87 and U251 cell lines.

**Supplementary materials legends**

**Additional file 1:**The details of experiments process in vitro

**Additional file 2: Table S1-S12.xlsx**

**Table S1** The 30 pyroptosis associated genes used for classification

**Table S2** Glioma classification pattern

**Table S3** GSVA enrichment analysis between these distinct pyroptosis-regulated clusters

**Table S4** The result of differential expression analysis (Cluster 2 vs Cluster 1)

**Table S5** Functional enrichment analyses of subclass differentially expressed genes (Cluster 2 vs Cluster 1)

**Table S6** Pathway enrichment analysis of differentially expressed genes from two subclasses

**Table S7** 15 identified pyroptosis-related signature genes in prognostic model

662 **Table S8** Differentially expressed genes from CGGA based on risk score

663 **Table S9** Differentially expressed genes from TCGA based on risk score

664 **Table S10** Differentially expressed lncRNA from TCGA based on risk score

665 **Table S11** Differentially expressed mir-RNA from TCGA based on risk score

666 **Table S12** Prognosis-related genes in the ceRNA network

667 **Table S13** Results of drug sensitivity based on 15 pyroptosis-related prognostic
668 signature genes

669 **Additional file 3:**

670 **Figure S1** Comparisons of different clinical parameters for pyroptosis-related genes.
671 **(A)** LGG and GBM. **(B)** WHO II vs WHOIII vs WHO IV. **(C)** IDH: mutations vs
672 wildtyp. **(D)**1p19_status: codel vs non-codel.

673 **Figure S2** Barplot of GO enrichment analysis for differentially expressed genes based
674 on subclasses.

675 **Figure S3** KEEG pathways analysis for differentially expressed genes based on
676 subclasses.

677 **Figure S4** Correlation of glioma subclasses with immune infiltration. **(A)** Immune cells.
678 **(B)** immune function

679 **Figure S5** Identification of 215 genes risk signature for OS by LASSO regression in
680 the CGGA cohort. (A) Forest plot of univariate cox regression of OS for 30 pyroptosis-
681 related genes. (B) Cross-validation for tuning parameters selection int the LASSO
682 regression. (C) LASSO regression of the 15 OS-related genes. (D) Heatmap showed
683 the association between risk group and clinical parameters and differentially expressed

684 genes of high- and low-risk group.

685 **Figure S6** Boxplot of risk score among different clinical characteristics. (A) Subclasses:
686 Cluster 1 vs Cluster 2. (B) Outcomes: Dead vs Alive. (C) Histology: GBM vs LGG. (D)
687 Grade: WHO II vs WHO III vs WHO IV. (E) 1p19q status: Codeletion vs non-
688 codeletion. (F) IDH status: Mutant wildtype.

689 **Figure S7** Subgroup analysis of OS based on risk score. **(A)** LGG. **(B)** GBM. **(C)** IDH
690 wildtype. **(D)** IDH mutation. **(E)** 1p9ql non-codel. **(F)** 1p9ql codel. **(G)** WHO II. **(H)**
691 WHO III. **(I)** WHO IV

692 **Figure S8** Comparisons of 15 signature genes among different immune subtype.

693 **Figure S9** Correlation of expression of 15 signature genes with cancer stem cell-like
694 properties (RNAss, DNAss) and TME (Stromal score, Immune score, and ESTIMATE
695 Score. (A) RNAss. (B) DNAss. (C) Stromal score. (D) Immune score. (E) ESTIMATE
696 score.

697 **Figure S10** Kaplan-Meier curves of lncRNAs for OS in the ceRNA network. **(A)**
698 AC025211.1. **(B)** AC068643.1. **(C)**ADH1L1-AS2. **(D)** CRNDE. **(E)** FAM181A-AS1.
699 **(F)** GDNF-AS1. **(G)** HOTAIRM1. **(H)** LINC00519 **(I)** MCF2L-AS1. **(J)** MIR210HG.
700 **(K)** NEAT1 **(L)**SLC6A1. **(M)** SNHG9.

701 **Figure S11** Forest plot of mRNAs for OS in the ceRNA network

702 **Figure S12** Kaplan-Meier curves of mir-RNAs for OS in the ceRNA network. **(A)** mir-
703 21. **(B)** mir-155. **(C)** mir-200a. **(D)** mir-216a. **(E)** mir-221. **(F)** mir-222. **(G)** mir-429.
704 **(H)** mir-503.

705 **Figure S13** The expression levels of identified prognostic genes between tumor and

706 normal

707

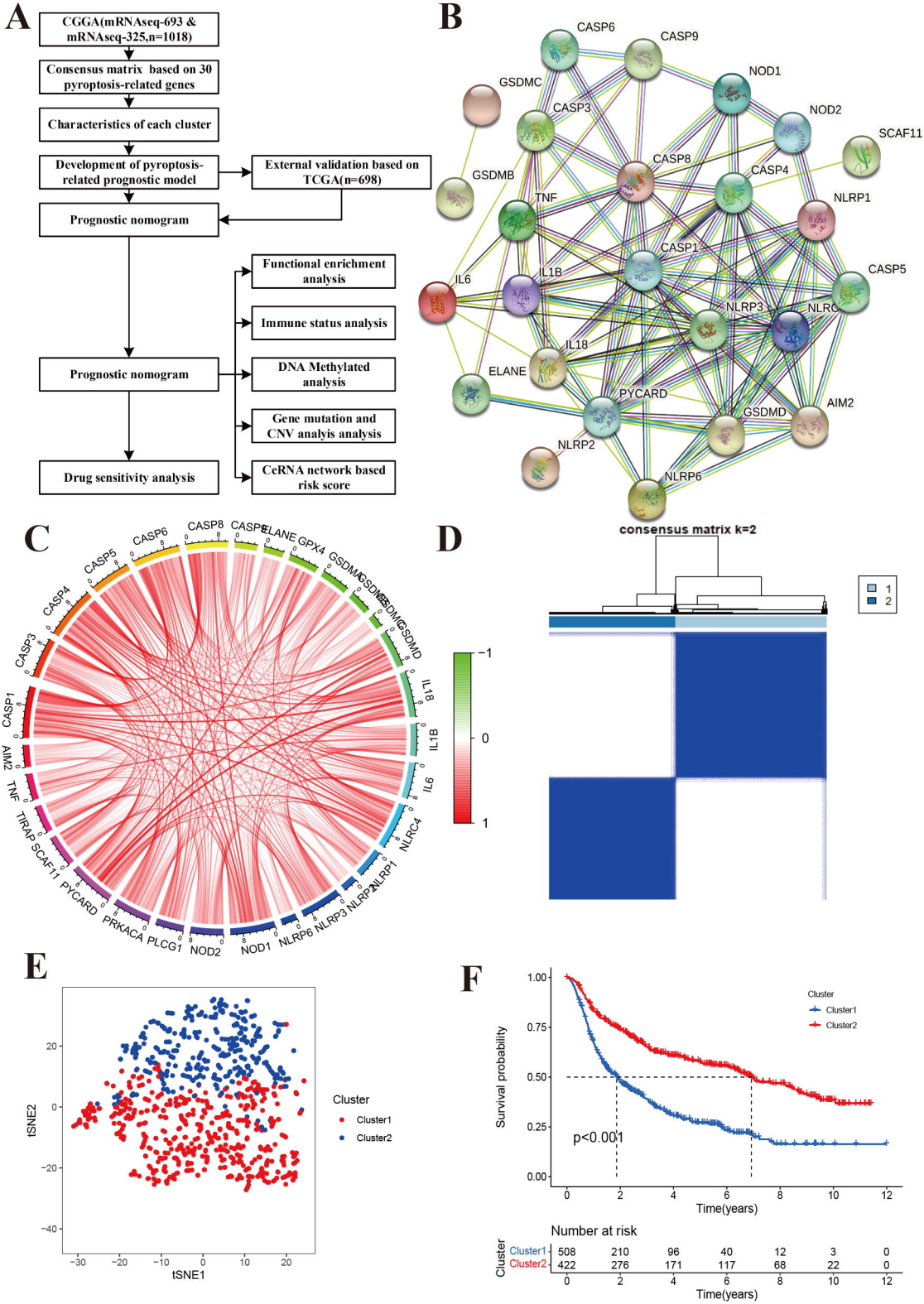
A
CGGA(mRNAseq-693 & mRNAseq-325,n=1018)
Consensus matrix based on 30 pyroptosis-related genes
Characteristics of each cluster
Development of pyroptosis-related prognostic model
External validation based on TCGA(n=698)
Prognostic nomogram
Prognostic nomogram
Functional enrichment analysis
Immune status analysis
DNA Methylated analysis
Gene mutation and CNV analyis analysis
Drug sensitivity analysis
CeRNA network based risk score
B
CASP6
CASP9
NOD1
GSDMC
CASP3
NOD2
SCAF11
CASP8
GSDMB
CASP4
TNF
NLRP1
CASP1
IL6
IL1B
CASP5
NLRP3
NLRC
IL18
ELANE
PYCARD
AIM2
GSDMD
NLRP2
NLRP6
C
CASP6
CASP8
CASP5
ELANE
GPX4
CASP4
GSDMA
GSDMB
GSDMC
GSDMD
CASP3
IL18
CASP1
IL1B
AIM2
IL6
TNF
NLRC4
TIRAP
SCAF11
NLRP1
PYCARD
NLRP2
PRKACA
NLRP3
PLCG1
NOD2
NLRP6
NOD1
D
consensus matrix k=2
1
2
−1
0
1
E
tSNE2
tSNE1
Cluster
Cluster1
Cluster2
F
Survival probability
p<0.001
Time(years)
Cluster
Cluster1
Cluster2
Number at risk
Cluster1 508 210 96 40 12 3 0
Cluster2 422 276 171 117 68 22 0
Time(years)

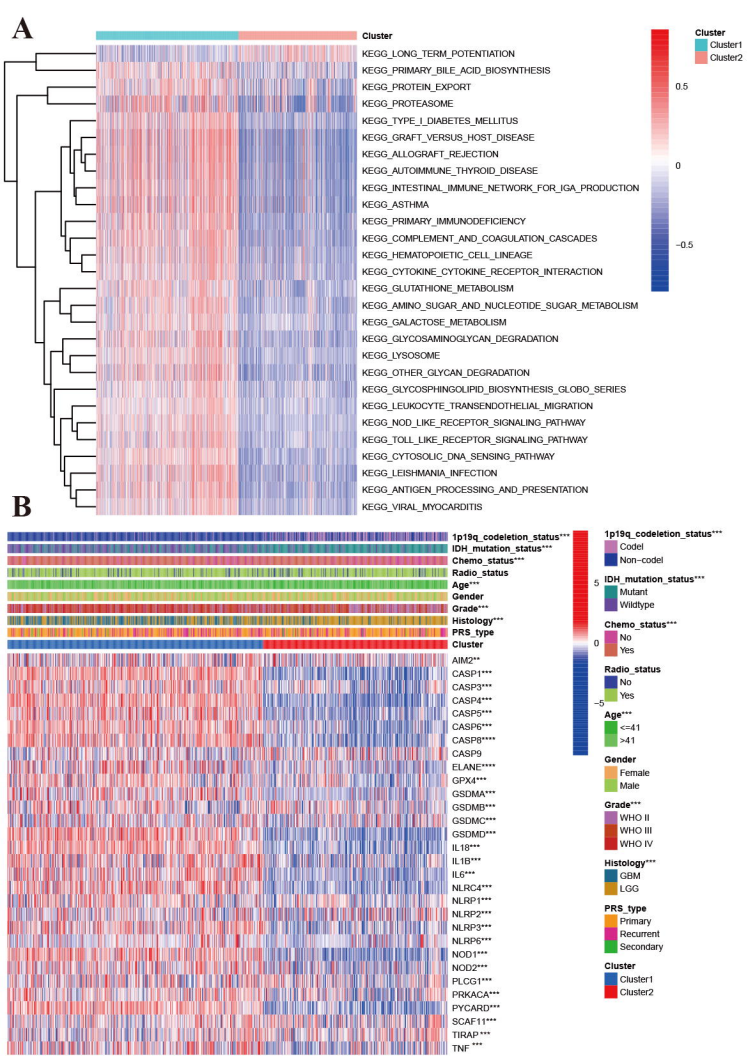
A
Cluster
KEGG_LONG_TERM_POTENTIATION
KEGG_PRIMARY_BILE_ACID_BIOSYNTHESIS
KEGG_PROTEIN_EXPORT
KEGG_PROTEASOME
KEGG_TYPE_I_DIABETES_MELLITUS
KEGG_GRAFT_VERSUS_HOST_DISEASE
KEGG_ALLOGRAFT_REJECTION
KEGG_AUTOIMMUNE_THYROID_DISEASE
KEGG_INTESTINAL_IMMUNE_NETWORK_FOR_IGA_PRODUCTION
KEGG_ASTHMA
KEGG_PRIMARY_IMMUNODEFICIENCY
KEGG_COMPLEMENT_AND_COAGULATION_CASCADES
KEGG_HEMATOPOIETIC_CELL_LINEAGE
KEGG_CYTOKINE_CYTOKINE_RECEPTOR_INTERACTION
KEGG_GLUTATHIONE_METABOLISM
KEGG_AMINO_SUGAR_AND_NUCLEOTIDE_SUGAR_METABOLISM
KEGG_GALACTOSE_METABOLISM
KEGG_GLYCOSAMINOGLYCAN_DEGRADATION
KEGG_LYSOSOME
KEGG_OTHER_GLYCAN_DEGRADATION
KEGG_GLYCOSPHINGOLIPID_BIOSYNTHESIS_GLOBO_SERIES
KEGG_LEUKOCYTE_TRANSENDOTHELIAL_MIGRATION
KEGG_NOD_LIKE_RECEPTOR_SIGNALING_PATHWAY
KEGG_TOLL_LIKE_RECEPTOR_SIGNALING_PATHWAY
KEGG_CYTOSOLIC_DNA_SENSING_PATHWAY
KEGG_LEISHMANIA_INFECTION
KEGG_ANTIGEN_PROCESSING_AND_PRESENTATION
KEGG_VIRAL_MYOCARDITIS
Cluster
Cluster1
Cluster2
0.5
0
−0.5
B
1p19q_codeletion_status***
IDH_mutation_status***
Chemo_status***
Radio_status
Age***
Gender
Grade***
Histology***
PRS_type
Cluster
AIM2**
CASP1***
CASP3***
CASP4***
CASP5***
CASP6***
CASP8***
CASP9
ELANE***
GPX4***
GSDMA***
GSDMB***
GSDMC***
GSDMD***
IL18***
IL1B***
IL6***
NLRC4***
NLRP1***
NLRP2***
NLRP3***
NLRP6***
NOD1***
NOD2***
PLCG1***
PRKACA***
PYCARD***
SCAF11***
TIRAP***
TNF***
5
0
−5
1p19q_codeletion_status***
Codel
Non−codel
IDH_mutation_status***
Mutant
Wildtype
Chemo_status***
No
Yes
Radio_status
No
Yes
Age***
<=41
>41
Gender
Female
Male
Grade***
WHO II
WHO III
WHO IV
Histology***
GBM
LGG
PRS_type
Primary
Recurrent
Secondary
Cluster
Cluster1
Cluster2

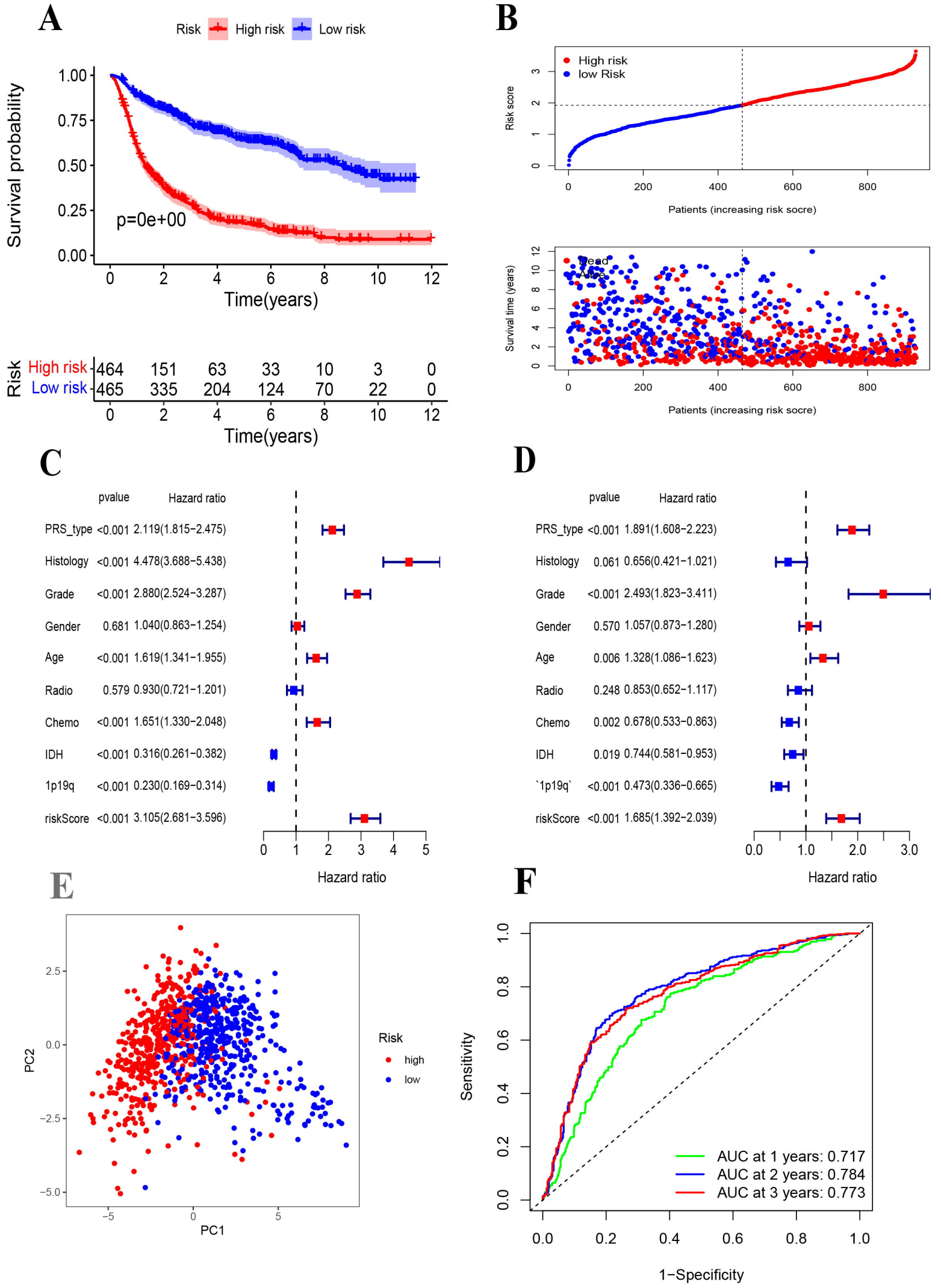
A
Risk
High risk
Low risk
Survival probability
1.00
0.75
0.50
0.25
0.00
p=0e+00
0
2
4
6
8
10
12
Time(years)
Risk
High risk 464 151 63 33 10 3 0
Low risk 465 335 204 124 70 22 0
Time(years)
B
High risk
low Risk
Risk score
Patients (increasing risk socre)
Dead
Alive
Survival time (years)
Patients (increasing risk socre)
C
pvalue
Hazard ratio
PRS_type <0.001 2.119(1.815−2.475)
Histology <0.001 4.478(3.688−5.438)
Grade <0.001 2.880(2.524−3.287)
Gender 0.681 1.040(0.863−1.254)
Age <0.001 1.619(1.341−1.955)
Radio 0.579 0.930(0.721−1.201)
Chemo <0.001 1.651(1.330−2.048)
IDH <0.001 0.316(0.261−0.382)
1p19q <0.001 0.230(0.169−0.314)
riskScore <0.001 3.105(2.681−3.596)
Hazard ratio
D
pvalue
Hazard ratio
PRS_type <0.001 1.891(1.608−2.223)
Histology 0.061 0.656(0.421−1.021)
Grade <0.001 2.493(1.823−3.411)
Gender 0.570 1.057(0.873−1.280)
Age 0.006 1.328(1.086−1.623)
Radio 0.248 0.853(0.652−1.117)
Chemo 0.002 0.678(0.533−0.863)
IDH 0.019 0.744(0.581−0.953)
`1p19q` <0.001 0.473(0.336−0.665)
riskScore <0.001 1.685(1.392−2.039)
Hazard ratio
E
PC2
PC1
Risk
high
low
F
Sensitivity
1−Specificity
AUC at 1 years: 0.717
AUC at 2 years: 0.784
AUC at 3 years: 0.773

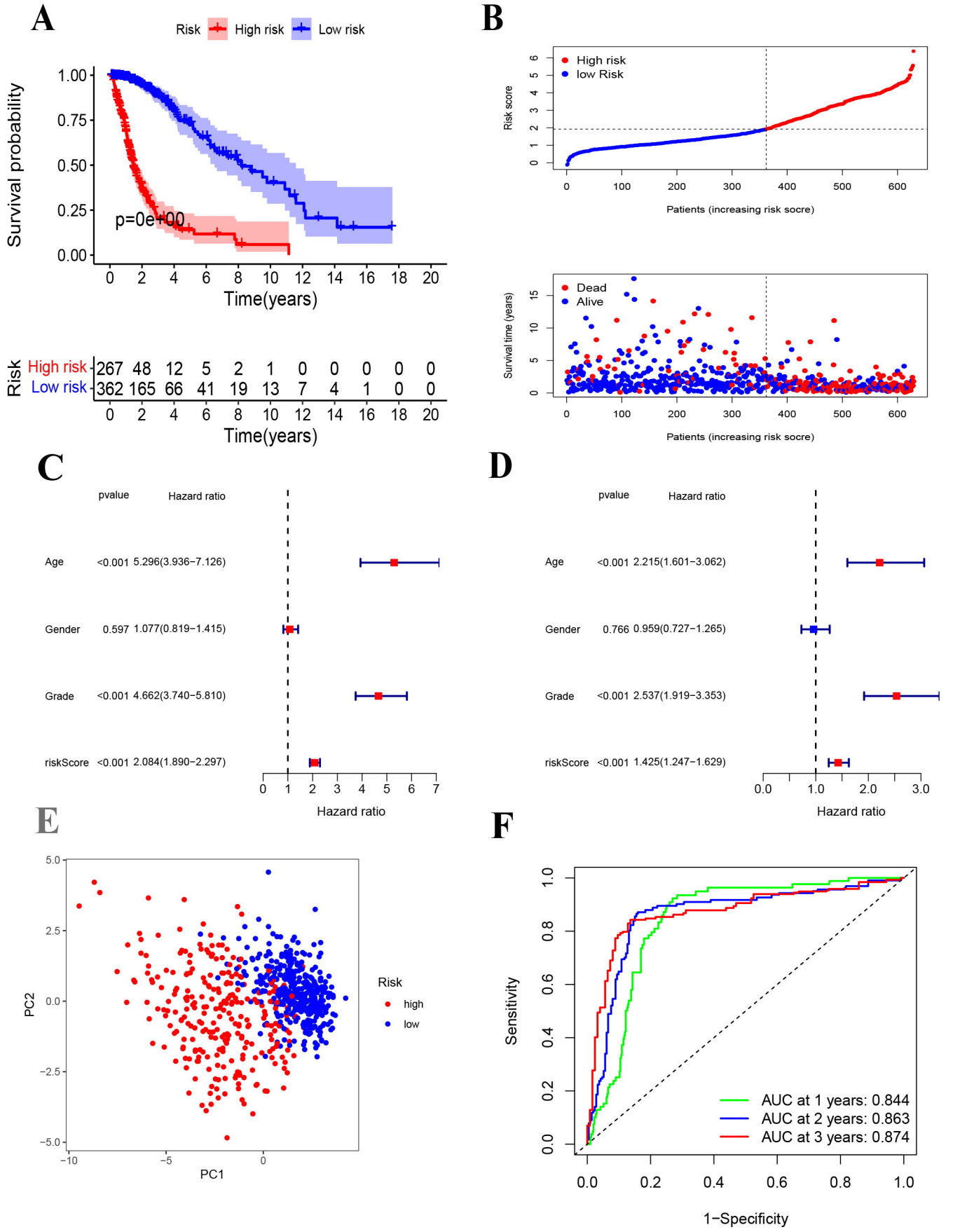
A
Risk
High risk
Low risk
Survival probability
1.00
0.75
0.50
0.25
0.00
p=0e+00
0 2 4 6 8 10 12 14 16 18 20
Time(years)
Risk
High risk 267 48 12 5 2 1 0 0 0 0 0
Low risk 362 165 66 41 19 13 7 4 1 0 0
0 2 4 6 8 10 12 14 16 18 20
Time(years)
B
High risk
low Risk
Risk score
0 1 2 3 4 5 6
0 100 200 300 400 500 600
Patients (increasing risk socre)
Dead
Alive
Survival time (years)
0 5 10 15
0 100 200 300 400 500 600
Patients (increasing risk socre)
C
pvalue
Hazard ratio
Age <0.001 5.296(3.936−7.126)
Gender 0.597 1.077(0.819−1.415)
Grade <0.001 4.662(3.740−5.810)
riskScore <0.001 2.084(1.890−2.297)
0 1 2 3 4 5 6 7
Hazard ratio
D
pvalue
Hazard ratio
Age <0.001 2.215(1.601−3.062)
Gender 0.766 0.959(0.727−1.265)
Grade <0.001 2.537(1.919−3.353)
riskScore <0.001 1.425(1.247−1.629)
0.0 1.0 2.0 3.0
Hazard ratio
E
5.0
2.5
0.0
−2.5
−5.0
PC2
−10 −5 0
PC1
Risk
high
low
F
Sensitivity
0.0 0.2 0.4 0.6 0.8 1.0
AUC at 1 years: 0.844
AUC at 2 years: 0.863
AUC at 3 years: 0.874
0.0 0.2 0.4 0.6 0.8 1.0
1−Specificity

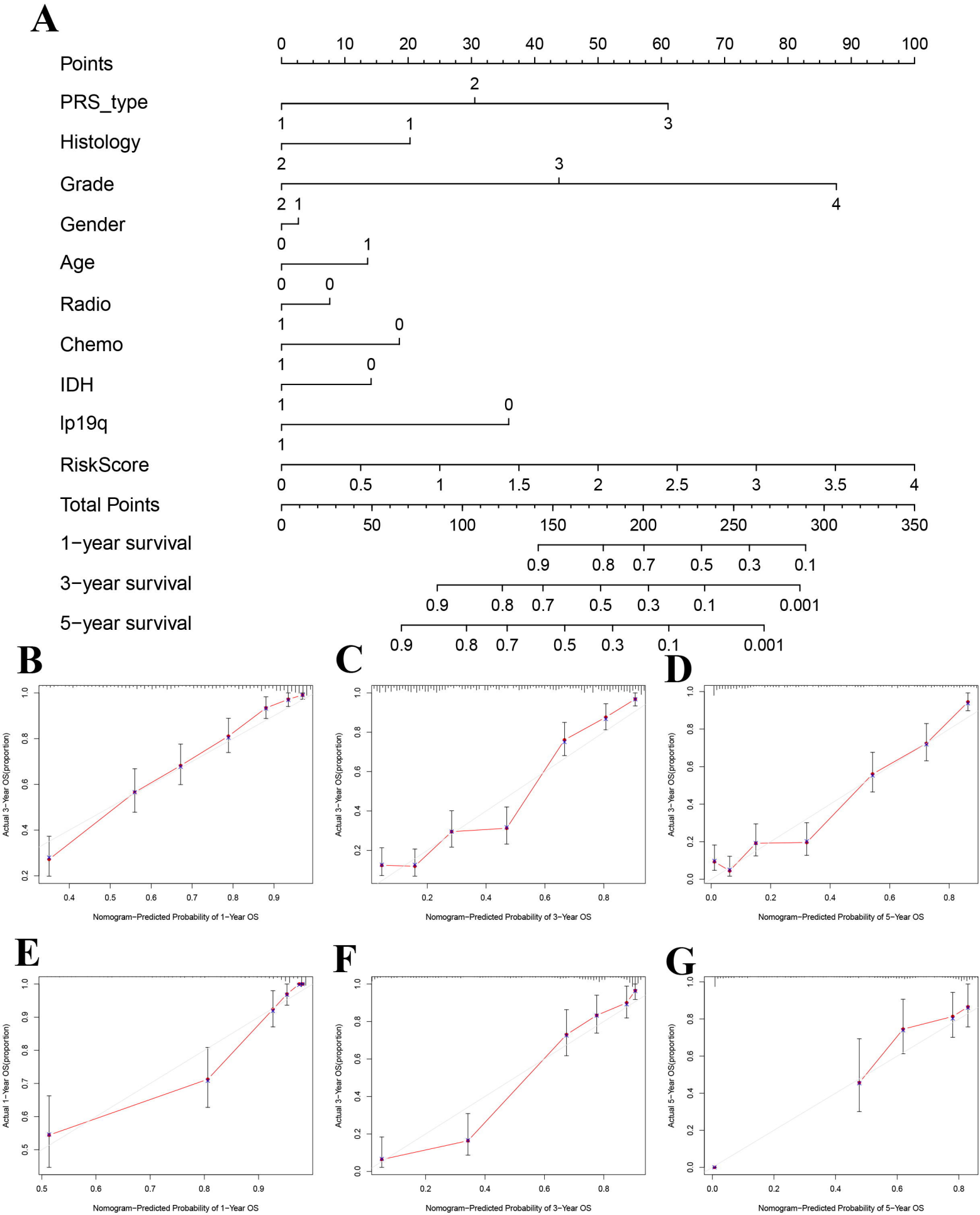
A
Points
PRS_type
Histology
Grade
Gender
Age
Radio
Chemo
IDH
1p19q
RiskScore
Total Points
1−year survival
3−year survival
5−year survival
B
C
D
E
F
G
Actual 3−Year OS(proportion)
Nomogram−Predicted Probability of 1−Year OS
Nomogram−Predicted Probability of 3−Year OS
Nomogram−Predicted Probability of 5−Year OS
Actual 1−Year OS(proportion)
Actual 5−Year OS(proportion)

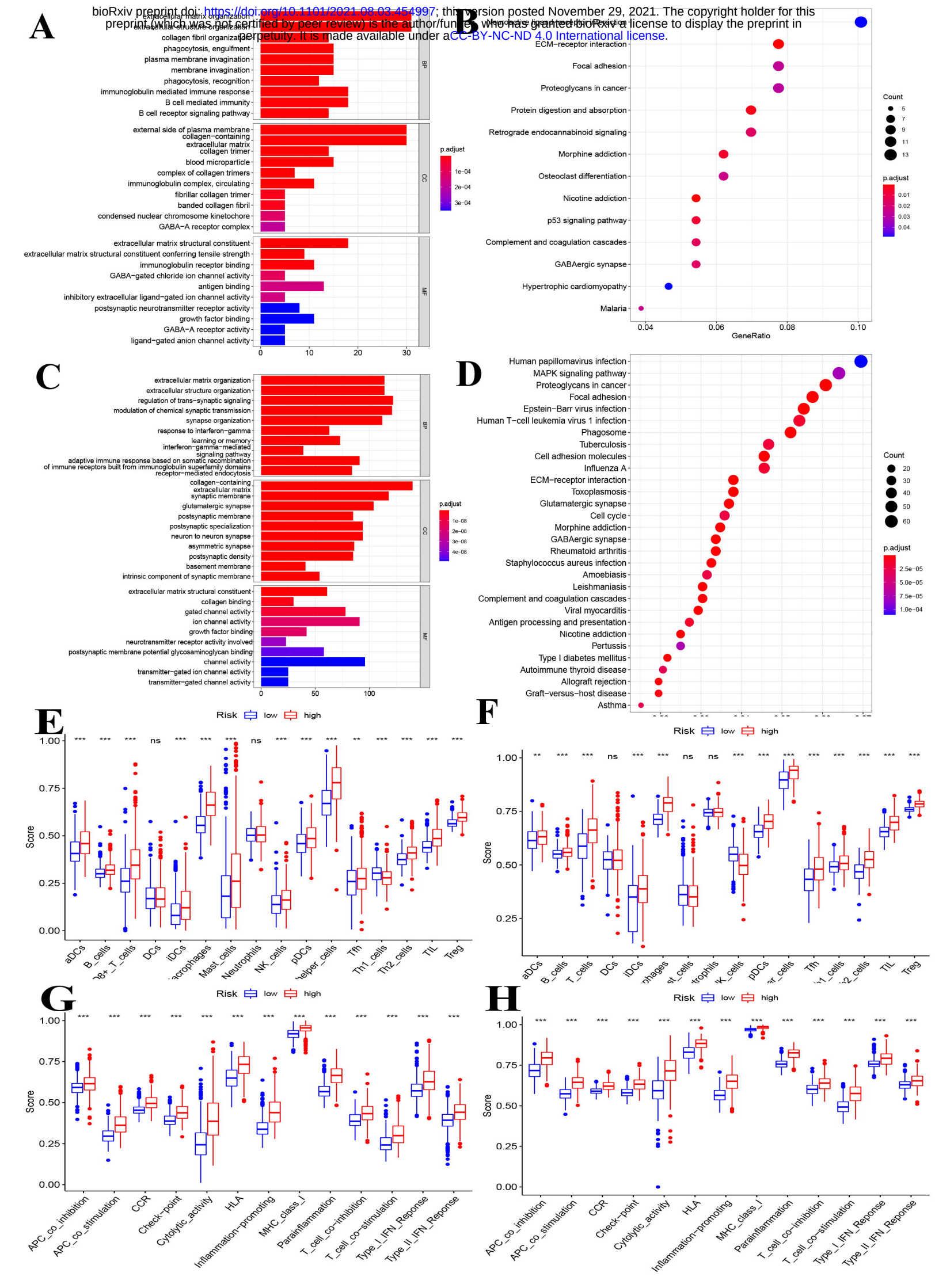

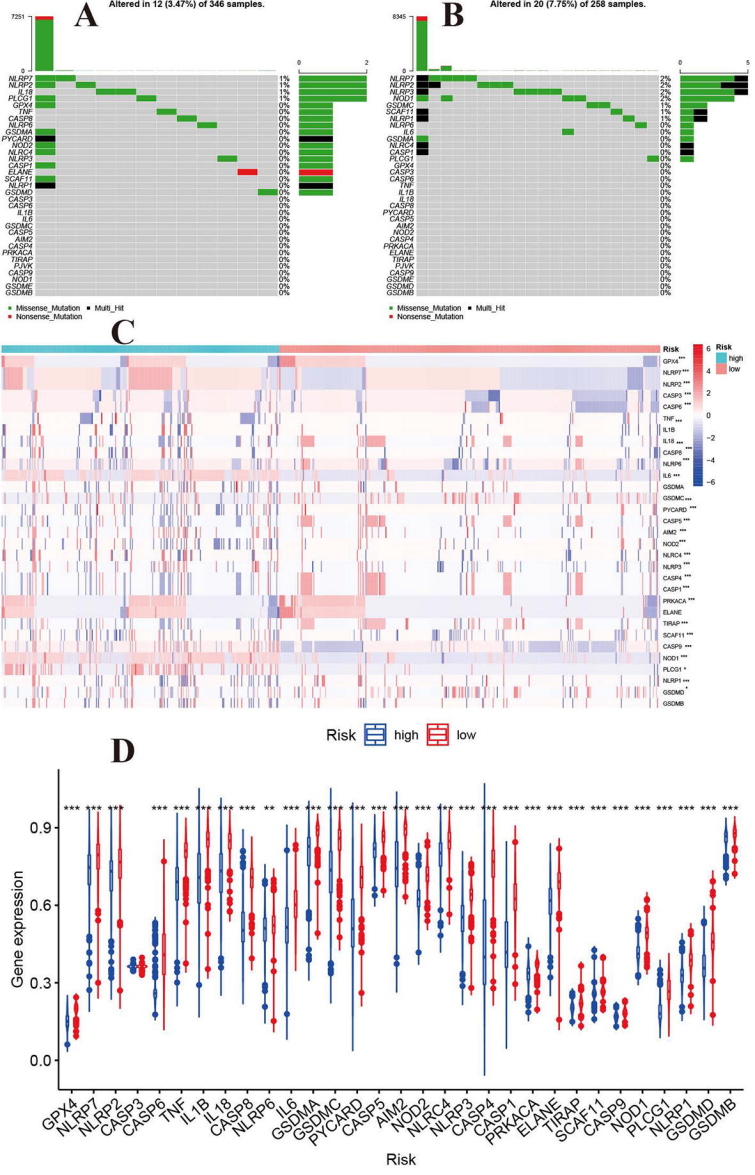
A
Altered in 12 (3.47%) of 346 samples.
NLRP7 1%
NLRP3 1%
IL18 1%
PLCG1 0%
GPX4 0%
TNF 0%
CASP8 0%
NLRP6 0%
GSDMA 0%
PYCARD 0%
NOD2 0%
NLRC4 0%
NLRP3 0%
CASP1 0%
ELANE 0%
SCAF11 0%
NLRP1 0%
GSDMD 0%
CASP3 0%
CASP6 0%
IL1B 0%
IL6 0%
GSDMC 0%
CASP5 0%
AIM2 0%
CASP4 0%
PRKACA 0%
TIRAP 0%
CASP9 0%
NOD1 0%
GSDME 0%
GSDMB 0%
Missense_Mutation
Nonsense_Mutation
Multi_Hit
B
Altered in 20 (7.75%) of 258 samples.
NLRP7 2%
NLRP3 2%
NLRP2 2%
CASP3 1%
GSDMC 1%
SCAF11 1%
NLRP1 1%
NLRP6 0%
IL6 0%
GSDMA 0%
NLRC4 0%
CASP1 0%
PLCG1 0%
GPX4 0%
CASP3 0%
CASP6 0%
TNF 0%
IL1B 0%
IL18 0%
CASP8 0%
PYCARD 0%
CASP5 0%
AIM2 0%
NOD2 0%
CASP4 0%
PRKACA 0%
ELANE 0%
TIRAP 0%
PLCG1 0%
CASP9 0%
GSDME 0%
GSDMD 0%
GSDMB 0%
Missense_Mutation
Nonsense_Mutation
Multi_Hit
C
Risk
high
low
GPX4 ***
NLRP7 ***
NLRP2 ***
CASP3 ***
CASP6 ***
TNF ***
IL1B
IL18 ***
CASP8 ***
NLRP6 ***
IL6 ***
GSDMA
GSDMC ***
PYCARD ***
CASP5 ***
AIM2 ***
NOD2 ***
NLRC4 ***
NLRP3 ***
CASP4 ***
CASP1 ***
PRKACA ***
ELANE
TIRAP ***
SCAF11 ***
CASP9 ***
NOD1 ***
PLCG1 **
NLRP1 ***
GSDMD *
GSDMB
Risk
high
low
D
Gene expression
0.0
0.3
0.6
0.9
GPX4 NLRP7 NLRP2 CASP3 CASP6 TNF IL1B IL18 CASP8 NLRP6 IL6 GSDMA GSDMC PYCARD CASP5 AIM2 NOD2 NLRC4 NLRP3 CASP4 CASP1 PRKACA ELANE TIRAP SCAF11 CASP9 NOD1 PLCG1 NLRP1 GSDMD GSDMB
Risk

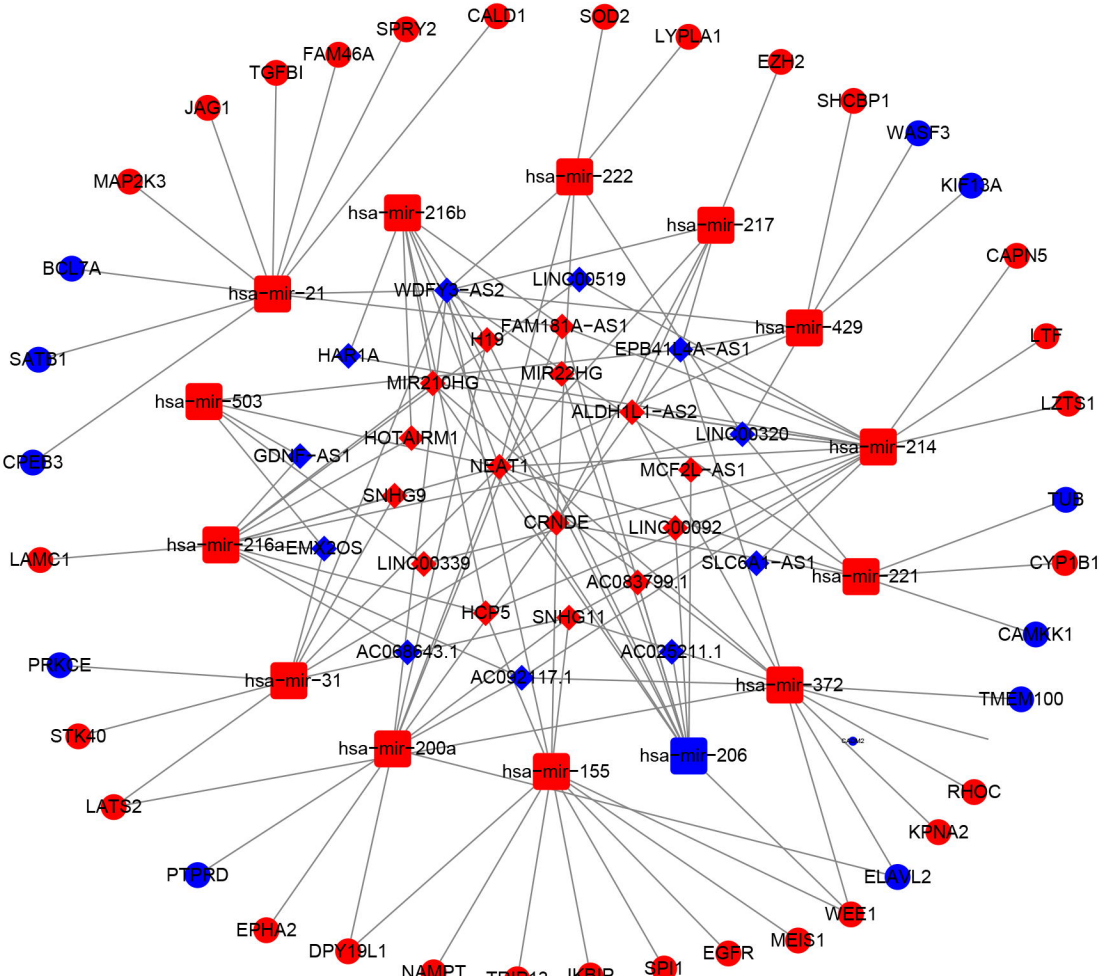
SPRY2
CALD1
SOD2
LYPLA1
FAM46A
TGFBI
EZH2
JAG1
SHCBP1
WASF3
MAP2K3
hsa-mir-222
KIF18A
hsa-mir-216b
hsa-mir-217
CAPN5
BCL7A
hsa-mir-21
LINC00519
WDFY3-AS2
FAM181A-AS1
hsa-mir-429
LTF
SATB1
H19
HAS1A
EPB41L4A-AS1
MIR210HG
MIR22HG
hsa-mir-503
LZTS1
ALDH1L1-AS2
HOTAIRM1
LINC00320
CPEB3
GDNF-AS1
hsa-mir-214
NEAT1
MCF2L-AS1
SNHG9
TUB
CRNDE
LINC00092
LAMC1
hsa-mir-216a
EMX2OS
LINC00339
SLC6A1-AS1
CYP1B1
AC083799.1
hsa-mir-221
HCP5
SNHG11
CAMKK1
AC068643.1
AC025211.1
PRKCE
hsa-mir-31
AC092117.1
hsa-mir-372
TMEM100
STK40
hsa-mir-200a
hsa-mir-206
hsa-mir-155
RHOC
LATS2
KPNA2
PTPRD
ELAVL2
WEE1
EPHA2
MEIS1
DPY19L1
EGFR
NAMPT
TRIP13
IKBIP
SPI1

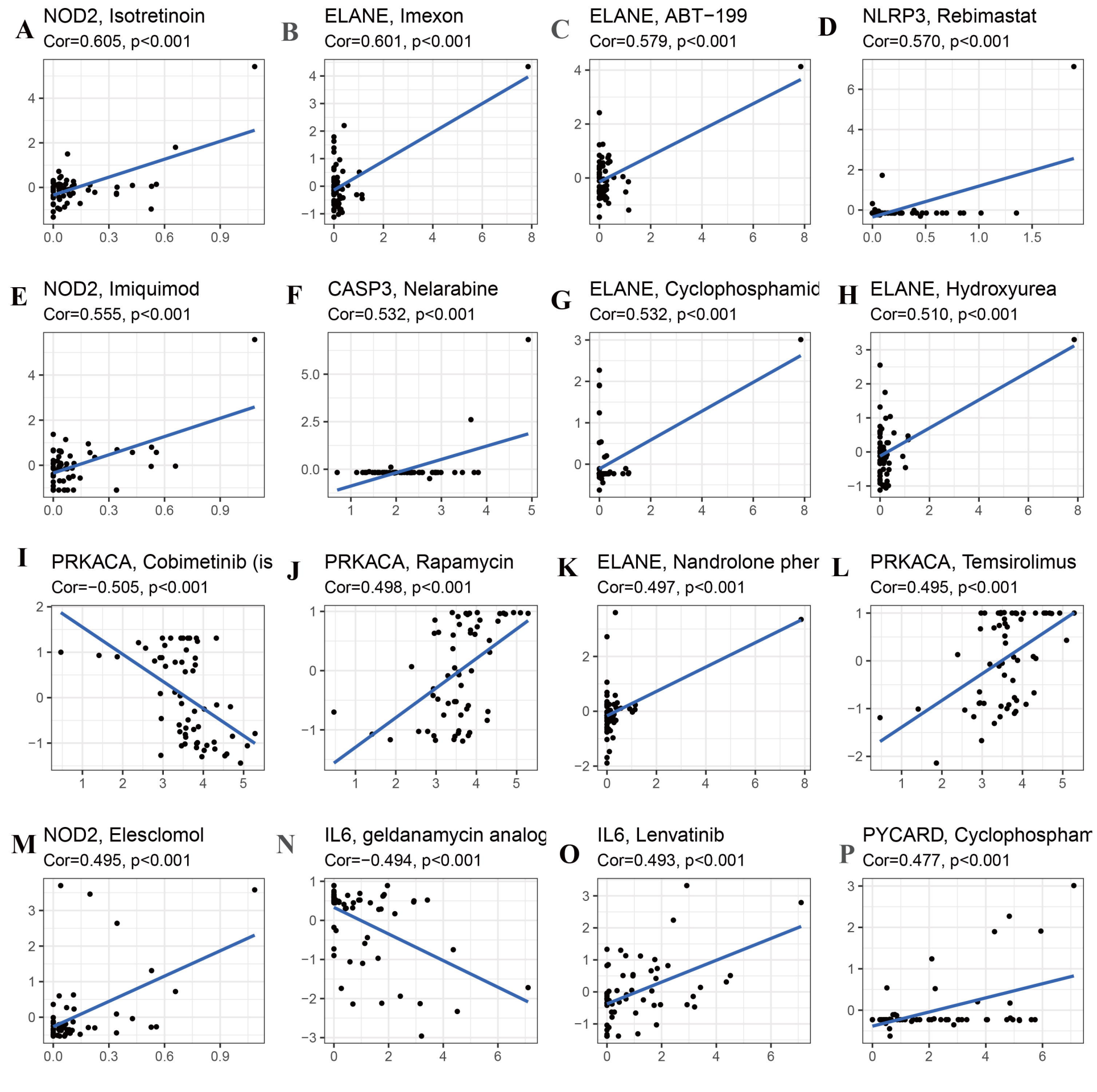
A
NOD2, Isotretinoin
Cor=0.605, p<0.001
B
ELANE, Imexon
Cor=0.601, p<0.001
C
ELANE, ABT−199
Cor=0.579, p<0.001
D
NLRP3, Rebimastat
Cor=0.570, p<0.001
E
NOD2, Imiquimod
Cor=0.555, p<0.001
F
CASP3, Nelarabine
Cor=0.532, p<0.001
G
ELANE, Cyclophosphamid
Cor=0.532, p<0.001
H
ELANE, Hydroxyurea
Cor=0.510, p<0.001
I
PRKACA, Cobimetinib (is
Cor=−0.505, p<0.001
J
PRKACA, Rapamycin
Cor=0.498, p<0.001
K
ELANE, Nandrolone pher
Cor=0.497, p<0.001
L
PRKACA, Temsirolimus
Cor=0.495, p<0.001
M
NOD2, Elesclomol
Cor=0.495, p<0.001
N
IL6, geldanamycin analog
Cor=−0.494, p<0.001
O
IL6, Lenvatinib
Cor=0.493, p<0.001
P
PYCARD, Cyclophospham
Cor=0.477, p<0.001

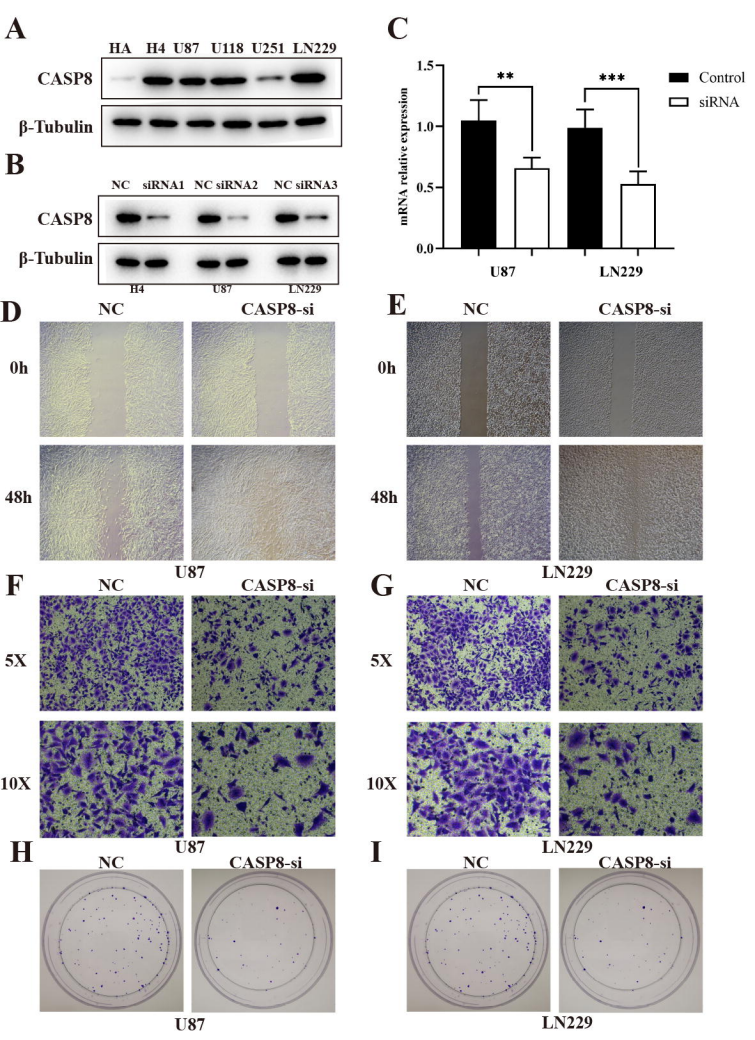
A
HA H4 U87 U118 U251 LN229
CASP8
β-Tubulin
B
NC siRNA1 NC siRNA2 NC siRNA3
CASP8
β-Tubulin
H4 U87 LN229
C
mRNA relative expression
1.5
1.0
0.5
0.0
**
***
Control
siRNA
U87 LN229
D
NC CASP8-si
0h
48h
U87
E
NC CASP8-si
0h
48h
LN229
F
NC CASP8-si
5X
10X
U87
G
NC CASP8-si
5X
10X
LN229
H
NC CASP8-si
U87
I
NC CASP8-si
LN229